Evgeny V. Nazarchuk, Oleg I. Siidra*, Dmitri O. Charkin and Yana G. Tagirova

Uranyl silicate nanotubules in $Rb_2[(UO_2)_2O(Si_3O_8)]$: synthesis and crystal structure

https://doi.org/10.1515/zkri-2023-0019
Received May 9, 2023; accepted August 10, 2023;
published online August 29, 2023

Abstract: A new rubidium uranyl silicate, $Rb_2(UO_2)_2O(Si_3O_8)$ (**1**), was obtained using high-temperature approach from the melt in silica tubes. Its crystal structure was solved by direct methods: hexagonal, $P6/m$, a = 27.7992(7), c = 7.2346(2) Å, V = 4841.8(3) Å^3, R_1 = 0.033. The structure of **1** represents a new structure type with unprecedented topology not observed before among U(VI) oxides and oxysalts. It is comprised of layers with large voids derived from the U_3O_8 structure formed exclusively by pentagonal $Ur O_5$ bipyramids. The low-occupied Rb sites are located in the interlayer space. The SiO_4 silicate tetrahedra in the structure of **1** share vertices to form rolled $[Si_6O_{16}]^{8-}$ chains. The nanotubules $[(UO_2)(Si_6O_{16})]^{6-}$ penetrate through both U_3O_8-derived layers and Rb interlayer. These tubules are attached to the U_3O_8 derived sheets via uranyl-uranyl interactions and edge-sharing between silicate tetrahedra and $Ur O_5$ bipyramids.

Keywords: inorganic synthesis; microporous structures; nanotubules; silicates; uranyl oxysalts

1 Introduction

Minerals of hexavalent uranium may form in the oxidation zones of uranium deposits [1]. They are also known as alteration products of spent nuclear fuel (SNF) [2]. Their study is therefore important both for mineralogy and materials science for the development of new functional materials [3]. Uranyl silicate minerals are formed at the earlier formation stages in the oxidation zones [4]. They are expected to play an essential role in the processes of radionuclide migration, accumulation, and deposition.

Among the synthetic compounds of hexavalent uranium, the species containing tetrahedral anions are most common and numerous. In their structures, uranium is generally coordinated by two oxygen atoms forming a uranyl cation (*Ur*). In the equatorial plane, it is coordinated from four to six ligands (e.g., O, Cl, Br, OH, H_2O, etc.) forming a tetra-, penta-, or hexagonal bipyramid. The anisotropy of bond lengths and blockage of apical coordination sites enhances the formation of chain and layered architectures, while framework structures are less common.

Several approaches to the synthesis of uranyl compounds are known including isothermal evaporation, hydrothermal treatment, as well as high temperature and salt flux synthesis [5]. Detailed structural topological analysis shows that synthesized uranium compounds often “inherit” structural complexes from the initial reagents. This phenomenon is illustratively demonstrated by uranyl selenates [6] and chromates [7] crystallizing from aqueous solutions.

In our experiments, we employed new synthesis techniques which permitted to prepare single crystals of a new uranyl silicate $Rb_2(UO_2)_2O(Si_3O_8)$ (**1**) described below.

2 Experimental

2.1 Synthesis

Caution! Although the uranium precursors used contain depleted uranium, standard safety measures for handling radioactive substances must be followed.

Yellow crystals of **1** (Figure 1) were produced in a high-temperature experiment. A mixture of 38 mg of RbCl (Vecton, 99.7 %), 20 mg U_3O_8 (Vecton, 98.7 %) and 110 mg PbO (Vecton, 99.5 %) was pre-dried at 80 °C. This mixture was transferred to a silica tube (which served also as the source of silicon), then 30 μL of 40 % hydrofluoric acid was injected to etch and so to activate the smooth inner surface of the tube. After 1 min, the tube was attached to a vacuum line, evacuated, and sealed. The silica tube was heated to 950 °C at a rate of 70 °C/h, soaked for 99 h, and cooled to room temperature at the rate of 5 °C/h. As the silica tube served as the silicon source, it was essentially attacked by the reaction medium, with some cristobalite present due to its devitrification. The crystalline silica formed thin off-white sheets weakly attached to the inner walls of the

***Corresponding author: Oleg I. Siidra**, Department of Crystallography, Saint-Petersburg State University, University emb. 7/9, St. Petersburg 199034, Russia; and Kola Science Center, Russian Academy of Sciences, Apatity, Murmansk Region, 184200, Russia, E-mail: o.siidra@spbu.ru
Evgeny V. Nazarchuk and Yana G. Tagirova, Department of Crystallography, Saint-Petersburg State University, University emb. 7/9, St. Petersburg 199034, Russia
Dmitri O. Charkin, Department of Chemistry, Moscow State University, Vorobievy Gory 1, bd. 3, Moscow 119991, Russia

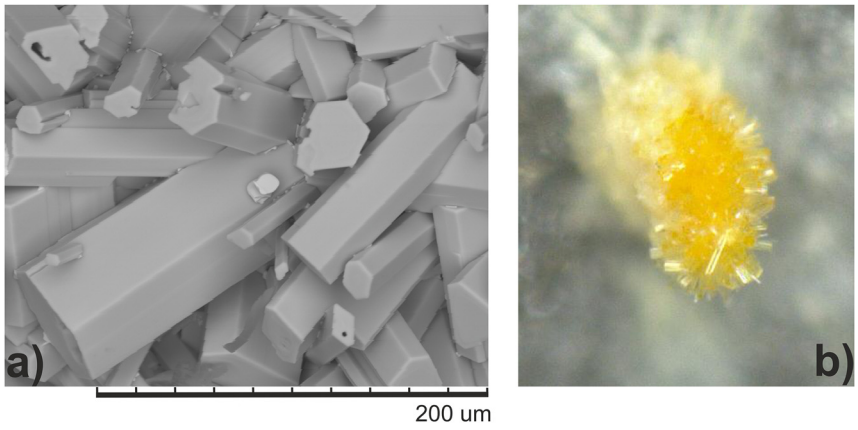

Figure 1: Hexagonal prismatic crystals of $Rb_2[(UO_2)_2O(Si_3O_8)]$. SEM image (a) and a photo under optical microscope (FOV 0.5 mm) (b).

tube which could be easily removed mechanically (by gentle blowing). The lead oxide has very likely assisted the formation of **1** by oxidizing U_3O_8 into U^{VI} and by attacking the inner surface of silica tube which proceeds very easily even below 400 °C in the presence of halides. Additional experiments have demonstrated that no reaction takes place between uranium oxides and intact silica tubes at much higher temperatures. Yet, the Pb^{2+} cations were not incorporated into **1**, as quantitative electron microprobe analysis (Hitachi S-3400N) revealed no other elements, except U, Si and Rb, with atomic number greater than 11 (Na). The averaged of 10 points gave the empirical formula calculated on the basis of 13 oxygen atoms per formula unit: $Rb_{2.02}(U_{1.02}O_2)_2O(Si_{2.93}O_8)$.

2.2 Single-crystal X-ray studies

Single crystal of **1** selected for X-ray diffraction analysis was glued onto glass filament and arranged in a Rigaku XtaLAB Synergy-S diffractometer equipped with a PhotonJet-S detector operating with MoKα radiation at 50 kV and 1 mA. More than a hemisphere of data was collected with a frame width of 0.5° in ω, and 60 s spent counting for each frame. The data were integrated and corrected for absorption applying a multiscan type model using the Rigaku Oxford Diffraction programs CrysAlis Pro. The experiment was performed at 150 K. The unit cell parameters were calculated by the least-squares method. The structure of **1** contains a number of low occupied Rb sites. The occupancies of Rb positions were first refined and adjusted on the final stages of the structure refinement to keep the formula electroneutral. The parameters of the X-ray diffraction experiment and structure refinement are given in Table 1. Crystallographic parameters are provided in Table 1 and selected interatomic distances in Table 2.

Table 1: Crystallographic data and refinement parameters for $Rb_2[(UO_2)_2O(Si_3O_8)]$.

Temperature (K)	150
Radiation	Mo*K*α
Crystal system	Hexagonal
Space group	*P6/m*
a (Å)	27.7992(7)
c (Å)	7.2346(2)
Volume (Å^3)	4841.8(3)
D_{calc} (g/cm^3)	3.866
μ (mm^{-1})	26.309
Crystal size (mm)	0.07 × 0.08 × 0.14
θ range (°)	3.174–27.996
h, *k*, *l* ranges	−33 → 35, −36 → 36, −9 → 9
Total reflections collected	4206
Unique reflections (R_{int})	3412(0.039)
$R_1[F > 4\sigma F]$, $wR_1[F > 4\sigma F]$	0.033, 0.075
R_{all}, wR_{all}	0.049, 0.080
Goodness-of-fit	1.053
CCDC number	2222967

3 Results

In the structure of **1**, three symmetrically independent uranium atoms are coordinated by five oxygen atoms each in the equatorial plane with the formation of *Ur*O_5 pentagonal bipyramids while U(4) atom forms *Ur*O_4 tetragonal bipyramid (Figure 2; Table 2). Four Si atoms are tetrahedrally coordinated and show no significant distortion.

The bond valence sums are 6.10, 6.03, 5.86, 6.09, 4.12, 4.15, 4.29, 4.18 for U(1)–U(4) and Si(1)–Si(4), respectively, which agree well to the formal valences of these atoms. Bond valences were calculated using the parameters of [8]. A minor overbonding for the silicon atoms is rather common among the structures of uranyl silicates [9]. Note that O16 vertex in $Si(3)O_4$ tetrahedron is split over O(16A) and O(16B) sites with 50 % occupancy each. The SiO_4 silicate tetrahedra in the structure of **1** share vertices to form rolled $[Si_6O_{16}]^{8-}$ chains (Figure 3). The double chains formed by alternating 4- and 6-membered tetrahedral rings were previously described in okenite $Ca_{10}Si_{18}O_{46}{\cdot}18(H_2O)$ [10] and yangite $PbMnSi_3O_8{\cdot}H_2O$ [11, 12]. $[Si_6O_{16}]^{8-}$ chains can be built from two wollastonite-type chains (Figure 3a). Both $[Si_6O_{16}]^{8-}$ chains in the structure of **1** and okenite are based upon the same arrangement of white nodes (Figure 3b and c), but the "… up–down … "

Table 2: Selected interatomic bonds in the structure of $Rb_2[(UO_2)_2O(Si_3O_8)]$.

U1–O1	1.798(6)	U3–O3	1.823(6)	Si1–O8	1.603(9)
U1–O1	1.798(6)	U3–O3	1.823(6)	Si1–O10	1.616(6)
<U1–O_{ap}>	**1.798**	**<U3–O_{ap}>**	**1.823**	Si1–O10	1.616(6)
U1–O6	2.195(9)	U3–O7	2.195(7)	Si1–O9	1.620(8)
U1–O8	2.269(8)	U3–O6	2.225(9)	**<Si1–O>**	**1.614**
U1–O11	2.318(8)	U3–O7	2.288(7)		
U1–O11	2.472(8)	U3–O9	2.468(8)	Si2–O12	1.606(6)
U1–O13	2.486(8)	U3–O8	2.737(9)	Si2–O12	1.606(6)
<U1–O_{eq}>	**2.348**	**<U3–O_{eq}>**	**2.383**	Si2–O11	1.609(9)
				Si2–O13	1.617(8)
U2–O2	1.801(6)	U4–O4	1.791(9)	**<Si2–O>**	**1.609**
U2–O2	1.801(6)	U4–O5	1.818(8)		
<U2–O_{ap}>	**1.801**	**<U4–O_{ap}>**	1.804	Si3–O14	1.570(7)
U2–O6	2.182(9)	U4–O14	2.222(7)	Si3–O16A	1.587(4)
U2–O9	2.294(8)	U4–O17	2.222(6)	Si3–O16B	1.699(9)
U2–O13	2.367(7)	U4–O14	2.222(7)	Si3–O12	1.614(6)
U2–O7	2.412(8)	U4–O17	2.222(6)	Si3–O15	1.609(6)
U2–O5	2.524(8)	**<U4–O_{eq}>**	**2.222**	**<Si3–O>**	**1.616**
<U2–O_{eq}>	**2.356**				
				Si4–O17	1.576(7)
				Si4–O10	1.608(6)
				Si4–O18	1.620(4)
				Si4–O15	1.625(6)
				<Si4–O>	**1.607**

Mean bond-length values are marked in bold.

orientations of the Si–O_t bonds relative to the plane of the chains are completely different.

Three *Ur*(3)O_5 polyhedra share common O7 vertices to form a *Ur*(3)$_3O_{12}$ trimer which further shares with three *Ur*(1)O_5 and three *Ur*(2)O_5 species via common edges thus forming a $[Ur_9O_{24}]^{30-}$ nonanuclear group (Figure 4a). Their condensation via common O–O edges leads to the formation of layers depicted in Figure 4b. $[Ur_9O_{24}]^{30-}$ nonanuclear group in the structure of **1** can be excised from the structure of U_3O_8 (*C*2*mm*) [13, 14] (Figure 4c).

Six rolled $[Si_6O_{16}]^{8-}$ double chains are linked via equatorial vertices of *Ur*(4)O_4 tetragonal bipyramids into tubular complexes (Figure 4d). The resulting topology can be described in the same way as performed previously for uranyl selenate [15] and uranyl sulfate [16] nanotubules. One has to dissect the tubular complex along its axis and to evolve it onto a plane (Figure 4e). The effective inner diameter of the tubule is 12.01 Å.

The interlayer and intratubular space are filled by partially occupied Rb sites (Figure 4f). The structure of **1** (Figure 4g) can be obtained from the ideal U_3O_8 (*C*2*mm*) structure according the following sequential transformations: (1) excision of $[Ur_9O_{24}]^{30-}$ nonanuclear groups and further condensation into hexagonal layers formed exclusively by

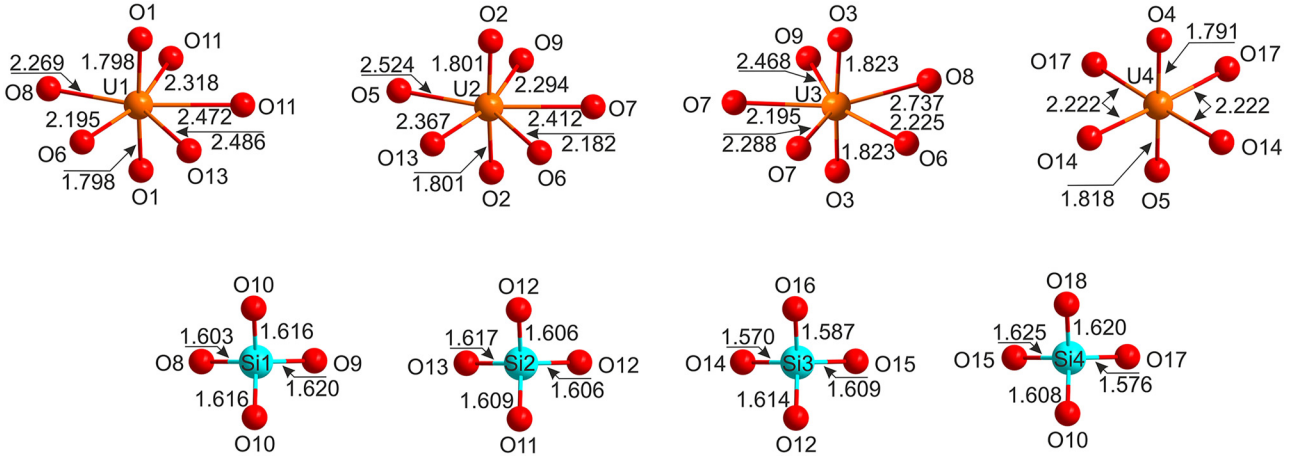

Figure 2: Coordination environments of U^{6+} and Si^{4+} cations in the structure of $Rb_2[(UO_2)_2O(Si_3O_8)]$.

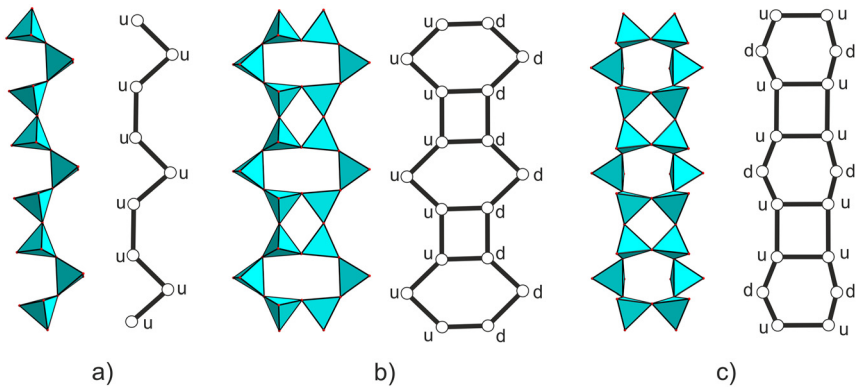

Figure 3: $[Si_3O_9]^{6-}$ chain in wollastonite $Ca_3(Si_3O_9)$ (a) $[Si_6O_{16}]^{8-}$ double chain in okenite $Ca_{10}Si_{18}O_{46}{\cdot}18(H_2O)$ (b) and rolled $[Si_6O_{16}]^{8-}$ double chain in $Rb_2[(UO_2)_2O(Si_3O_8)]$ (c) and their nodal representations.

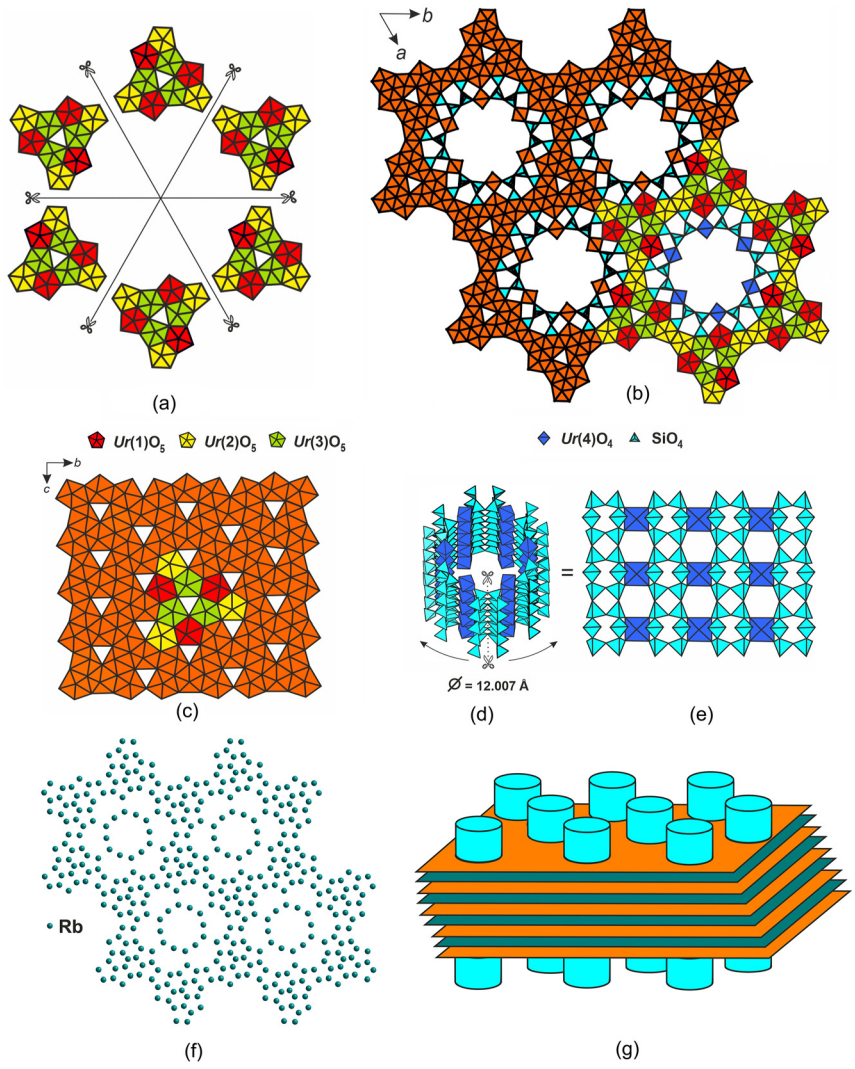

Figure 4: Condensation of the uranium polyhedra with the formation of the nonanuclear $[Ur_9O_{24}]^{30-}$ groups (a) and their further condensation into layers (b) in the structure of $Rb_2[(UO_2)_2O(Si_3O_8)]$. U_3O_8 (*C*2*mm*) archetype layer with the highlighted $[Ur_9O_{24}]^{30-}$ group (c). Polyhedral representation of the uranyl silicate nanotubule with inner diameter 12.01 Å (d). *Ur*(4)O_4 and SiO_4 tetrahedra are shown in dark blue and light blue, respectively. Notionally, the tubule can be unfolded into layer (e) composed of corrugated $[Si_6O_{16}]^{8-}$ single chains and isolated *Ur*(4)O_4 polyhedra. The interlayer and intratubular space filled by partially occupied Rb sites (f). The overall scheme of the structure of $Rb_2[(UO_2)_2O(Si_3O_8)]$ composed of U_3O_8-derived layers (orange sheets), disordered Rb nets (blue sheets) and $[(UO_2)(Si_6O_{16})]^{6-}$ nanotubules (blue cylinders) (g).

pentagonal *Ur*O_5 bipyramids; (2) intrusion of Rb into the interlayer space; (3) insertion of $[(UO_2)(Si_6O_{16})]^{6-}$ complexes which penetrate through both U_3O_8-derived layers and Rb interlayer.

4 Concluding remarks

The structure of **1** represents a new structure type with unprecedented topology not observed before in U(VI) oxides and oxysalts. Nanotubular (NT) motifs [17] were observed previously in several uranyl selenates and sulfates [15, 16] and borate phosphates [18]. Heteropolyhedral tubular architectures are still exceptionally rare among uranyl compounds. However, tubular silicate complexes are well known in minerals and synthetic compounds [11] due to the flexibility of the silicate anion. The rolled $[Si_6O_{16}]^{8-}$ double chains in **1** are topologically different (Figure 3) from those previously described in okenite and yangite.

It is also rare for the uranyl oxygen atoms to be involved in bonding interactions with other uranyl centers. This phenomenon is called a uranyl–uranyl (i.e., cation–cation) interaction. In the structure of **1**, it is observed between uranyl ions of the U(4) and U(2) atoms (Figure 5).

The O(5) atom of the U(4)O_2 uranyl group is bonded also to the U(2) atom, whereas O(4) atom is weakly bonded to Rb atoms. Four O14 atoms in the equatorial plane of the *Ur*(4)O_4 bipyramid are shared with the silicate tetrahedra. Thus $[(UO_2)(Si_6O_{16})]^{6-}$ tubules are attached to the U_3O_8 derived sheet via uranyl-uranyl interactions and edge-sharing between silicate tetrahedra and *Ur*O_5 bipyramids as shown in Figure 5. Layers in U_3O_8 are archetypic to a large number of different topologies [19] both in minerals and inorganic compounds. The use of structure building units (SBU) in

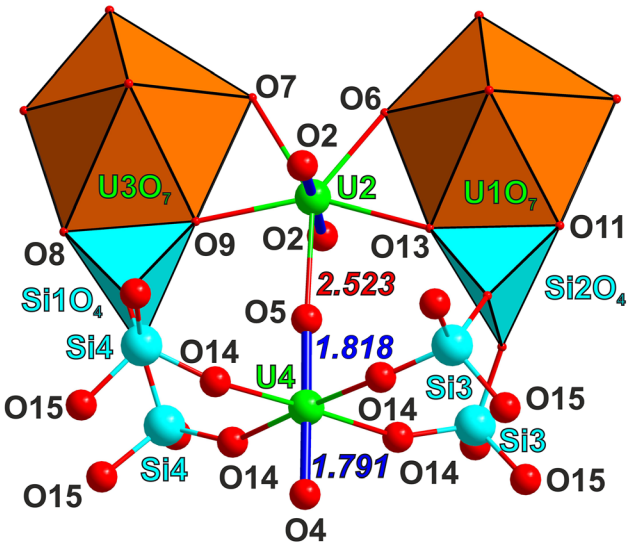

Figure 5: Polyhedral and ball-and-stick representation of the connectivity modes in $Rb_2(UO_2)_2O(Si_3O_8)$. Uranyl oxygen bonds are shown with blue bold lines.

uranium oxides is not uncommon for the crystal engineering of new complex uranyl oxysalts.

It is also worth noting that synthesis of uranyl silicates is strongly enhanced by the presence of "activators", PbO and halides in this case. The underlying chemical processes are yet obscure and demand further studies which are partially underway. We consider a likely sequence of reactions starting from attacking the silica surface by HF and low-melting lead oxychlorides formed upon early stages of heating. At higher temperatures, PbO also readily attacks silica. Formation of various volatile species like SiF_4 or $SiCl_4$ is also rather likely at higher temperatures. All this can be considered as "chemical activation" of fused silica tube with an initially very small and smooth surface area and expected low reactivity. The presence of solidified metallic droplets in the products suggests oxidation, at least partial, of U_3O_8 by PbO or initially formed lead silicates; concomitant disproportionation of U^V from U_3O_8 into U^{IV} and U^{VI} in the presence of silica, which is an acidic oxide, also cannot be completely ruled out (known compounds of $U^VO_2^+$ are formed in basic conditions and contain extra O^{2-} or OH^- anions). Note that presence of various fluxing media also essentially enhances formation of a multitude of various species. Evidently, use of other silica "activators" is very likely to bring new complex and elegant uranyl silicate structures.

Acknowledgments: Technical support by the X-Ray Diffraction and Geomodel Resource Centers of Saint-Petersburg State University is gratefully acknowledged.
Research ethics: Not applicable.
Author contributions: The authors have accepted responsibility for the entire content of this manuscript and approved its submission.
Competing interests: The authors state no conflict of interest.
Research funding: This work was financially supported by the Russian Science Foundation through the grant 23-27-00153 (E.V.N. and Y.G.T.).
Data availability: The raw data can be obtained on request from the corresponding author.

References

1. Hazen R. M., Ewing R. C., Sverjensky D. A. Evolution of uranium and thorium minerals. *Am. Mineral.* 2009, *94*, 1293–1311.
2. Finch R. J., Buck E. C., Finn P. A., Bates J. K. Oxidative corrosion of spent UO_2 fuel in vapor and dripping groundwater at 90 °C. *MRS Symp. Proc.* 1999, *556*, 431–438.
3. Burns P. C., Ikeda Y., Czerwinski K. Advances in actinide solid-state and coordination chemistry. *MRS Bull.* 2010, *35*, 868–876.
4. Belova L. N., Doynikova O. A. Formation conditions of uranium minerals in oxidation zone of uranium deposits. *Geol. Ore Deposits* 2003, *45*, 130–132.
5. Morrison G., zur Loye H. C. Flux growth of $[NaK_6F][(UO_2)_3(Si_2O_7)_2]$ and $[KK_6Cl][(UO_2)_3(Si_2O_7)_2]$: the effect of surface area to volume ratios on reaction products. *Cryst. Growth Des.* 2016, *16*, 1294–1299.
6. Krivovichev S. V., Gurzhiy V. V., Tananaev I. G., Myasoedov B. F. Uranyl selenates with organic templates: principles of structure and characteristics of self-organization. *Russ. J. Gen. Chem.* 2009, *79*, 2723–2730.
7. Siidra O. I., Nazarchuk E. V., Suknotova A. N., Kayukov R. A., Krivovichev S. V. Cr(VI) trioxide as a starting material for the synthesis of novel zero-one-and two-dimensional uranyl dichromates and chromate-dichromates. *Inorg. Chem.* 2013, *52*, 4729–4735.
8. Gagné O. C., Hawthorne F. C. Comprehensive derivation of bond-valence parameters for ion pairs involving oxygen. *Acta Crystallogr. B Struct. Sci.* 2015, *71*, 562–578.
9. Nazarchuk E. V., Siidra O. I., Charkin D. O., Tagirova Y. G. Microporous uranyl silicates: a new route for the synthesis of mineral like representatives. *Materials* 2023, *16*, 4153.
10. Merlino S. Okenite, $Ca_{10}Si_{18}O_{46}{\cdot}18(H_2O)$: the first example of a chain and sheet silicate. *Am. Mineral.* 1983, *68*, 614–622.
11. Day M. C., Hawthorne F. C. A structure hierarchy for silicate minerals: chain, ribbon, and tube silicates. *Mineral. Mag.* 2020, *84*, 165–244.
12. Downs R. T., Pinch W. W., Thompson R. M., Evans S. H., Megaw L. Yangite, $PbMnSi_3O_8{\cdot}H_2O$, a new mineral species with double wollastonite silicate chains, from the Kombat mine, Namibia. *Am. Mineral.* 2016, *101*, 2539–2543.
13. Baenziger N. C. The crystal structures of some thorium and uranium compounds. *Iowa State Coll. J. Sci.* 1952, *27*, 126–128.
14. Zhang F. X., Lang M., Wang J. W., Li W. X., Sun K., Prakapenka V., Ewing R. C. High-pressure U_3O_8 with the fluorite-type structure. *J. Solid State Chem.* 2014, *213*, 110–115.
15. Krivovichev S. V., Tananaev I. G., Kahlenberg V., Kaindl R., Myasoedov B. F. Synthesis, structure, and properties of inorganic nanotubes based on uranyl selenates. *Radiochemistry* 2005, *47*, 525–536.

16. Siidra O. I., Nazarchuk E. V., Charkin D. O., Chukanov N. V., Depmeier W., Bocharov S. N., Sharikov M. I. Uranyl sulfate nanotubules templated by N-phenylglycine. *Nanomaterials* 2018, *8*, 216–225.
17. Nazarchuk E. V., Charkin D. O., Siidra O. I., Kalmykov S. N. Organically templated layered uranyl molybdate $[C_3H_9NH^+]_4[(UO_2)_3(MoO_4)_5]$ structurally based on mineral-related modular units. *Minerals* 2020, *10*, 659.
18. Wu S., Wang S., Diwu J., Depmeier W., Malcherek T., Alekseev E. V., Albrecht-Schmitt T. E. Complex clover cross-sectioned nanotubules exist in the structure of the first uranium borate phosphate. *Chem. Commun.* 2012, *48*, 3479–3481.
19. Dal Bo F., Aksenov S. M., Burns P. C. $Mg[(UO_2)_2(Ge_2O_6(OH))_2]\cdot(H_2O)_{4.4}$, a novel compound with mixed germanium coordination: cation disordering and topological features of β-U_3O_8 type sheets. *Z. Kristallogr.* 2019, *234*, 383–393.